MDPI

Article

Heat Treatment of Calcite to Enhance Its Removal of Color Dye Alizarin Red S

Zhaohui Li [1,*], Anna Bowman [1], Angie Rayniak [1], Jadyn Strommen [1], Lori Allen [2] and Shangping Xu [3]

[1] Department of Geosciences, University of Wisconsin—Parkside, 900 Wood Road, Kenosha, WI 53144, USA
[2] Department of Chemistry, University of Wisconsin—Parkside, 900 Wood Road, Kenosha, WI 53144, USA
[3] Department of Geosciences, University of Wisconsin Milwaukee, 3209 N. Maryland Ave., Milwaukee, WI 53211, USA
* Correspondence: li@uwp.edu

Abstract: The use of color dyes in modern society presents a great challenge to the environment. Thus, extensive studies have been conducted in the last 30 years on the removal of color dyes from aqueous solutions such industrial wastewater. In this study, the removal of alizarin red S (ARS), an anionic dye, from solution by raw calcite (Cal) and heat-treated calcite (HCal) was conducted and compared under different physico-chemical conditions. Based on the isotherm study, the ARS removal capacities increased from 167 to 251 mmol/kg after the Cal was heated to 1000 °C for 3 h. The X-ray diffraction analyses showed no difference in the calcite phase between Cal and HCal after ARS sorption. Fourier-transform infrared results also showed no change in the calcite phase after ARS sorption, except a slightly increase in wavenumber from 713 to 727 cm^{-1} for the OCO bending of HCal at high ARS sorption levels. SEM observations showed about the same particle size and morphology before and after ARS sorption. The TGA data showed the formation of CaO after Cal was heated, and CaO converted back into calcite after being in contact with water or ARS solution for 24 h and then being air-dried. Thus, the high ARS removal could be due to CaO produced after Cal being heated. The findings from this research proved that there is great potential in the use of calcite, a low-cost and readily available Earth material, after heat treatment for the removal of contaminants from water.

Keywords: calcite; color dyes; enhancement; heat treatment; removal; sorption

1. Introduction

In today's society, about 1.6 million tons of dyes are produced annually and used in industries including textile, paper, plastics, marine, culinary, paints, and coatings [1]. Just in the textile industry alone, after the dyeing processes are finished, the leftover dye discharged into the environment may be as high as 85% of the initial dye [2], which accounts for the major driving force behind studies for dye removal over the last several decades. Mechanistically speaking, the removal of dyes could be achieved through physical, chemical, and biological processes [2]. For the physical removal of color dyes from solution, sorption is a simple yet effective method provided that the sorbents are inexpensive in material cost, have a wide availability, and have a high removal capacity. Earth materials, due to their low material cost and high material reserves, have attracted great attention for the removal of color dyes [3,4].

Dyes are classified as cationic, anionic, nonionic, and zwitterionic depending on their charges in solution. As most Earth materials bear negative charges on their surfaces, they have great potential for the removal of cationic dyes from solution [5], although the removal of zwitterionic and anionic dyes by clay minerals has also been studied [6–8].

Alizarin red S (ARS) is an anionic dye. Originally, it was derived from the roots of plants of the madder genus, and structure-wise, it is made of typical dihydroxyanthraquinone [9]. Initially, ARS was used for the identification of carbonate minerals [10].

Later, it was found that ARS stain on certain carbonate minerals such as aragonite, calcite, witherite, and cerussite was more obvious, as these minerals dissolve more rapidly in a dilute hydrochloric acid system. In contrast, dolomite, siderite, magnesite, and rhodochrosite reacted much slower with the acid and could not be stained by ARS [11]. In comparison to carbonated minerals, ARS sorbed more on apatite, and the OH groups rather than the $-SO_3$ group were responsible for ARS sorption [12].

ARS was also studied for the determination of aluminum content in silicates, as the reaction between aluminum and ARS requires two ARS molecules to form complexation with one atom of aluminum [13]. Later, a patent was granted for the determination of Al(III) by ARS [14]. However, at pH 4.55, the presence of Ca^{2+} could form a complex between Ca^{2+} and ARS, which would affect the quantification of Al(III) [15]. The formation of ARS with Ca^{2+} explained why ARS was used for Ca stain [16]. In biology, ARS staining has been used to evaluate calcium-rich deposits in cells. This staining method is particularly versatile, as the dye can be extracted from the stained monolayer and assayed [17]. Potentiometric titration showed that $Ca(HARS)_2^{2-}$ dominated at pH 5 to 8 and $CaARS^-$ was the major species at pH > 8 [18]. Also, on surface of CaF_2, the complexation of ARS with Ca^{2+} could also form [19]. In addition to Ca, ARS may also react with Mg and complex with other divalent transition metals [9].

Due to its anionic nature, materials for ARS removal are mostly organic as well as synthetic carbon nanotubes [20]. An activated carbon with a mesh size of 40–60 and surface area of 300 m^2/g was tested for the removal of ARS, and the calculated ARS sorption capacity was ~7 mg/g based on the Langmuir sorption isotherm model [21]. For inorganic materials, calcium hydroxide was tested for the removal of ARS under different physical and chemical conditions, but no ARS sorption capacity was provided [22]. Additionally, talc was coated with magnetite nanoparticles to enhance ARS removal with a capacity of 12 mg/g [23]. ARS removal from aqueous solution was also evaluated under different physical and chemical conditions using alumina, but the removal capacity was not mentioned [20]. A bentonite in sodium form was tested for ARS removal under different physico-chemical conditions with an ARS sorption capacity at 170 mg/g [24]. ARS removal was also tested using layered double hydroxide (LDH) due to its net positive charges on the surfaces [25]. In most of these studies, the mechanism of ARS removal was not discussed.

In addition to the use of raw materials for ARS removal, inorganic materials were also modified to enhance ARS removal. For instance, activated clay was modified by iron oxide to enhance the ARS removal capacity, but no comparison was made with the clay without iron oxide modification, and the X-ray diffraction (XRD) data showed that the dominant mineral was quartz, not clay mineral at all [26]. A composite material made of Fe_2O_3-coated biochar/kaolin showed ARS removal. Although the biochar and Fe_2O_3-coated biochar were tested as the controls, the kaolin alone was not evaluated for the comparison [27].

The mechanism of ARS sorption on clinoptilolite, a zeolite group mineral, was attributed to ligand formation between the Ca^{2+} on clinoptilolite surfaces and the O on the second carbon of ARS or the O with SO_3, as the ARS removal capacity was 92 mmol/kg, close to the external cation exchange capacity of the mineral, and results from molecular dynamic simulations suggested aggregations and dimer formations on the mineral surfaces [4].

In addition to the previously mentioned minerals, carbonated minerals such as calcite (Cal) and dolomite (Dol) were also evaluated for their removal of color dyes before and after heat treatment. For example, Dol heated to 800 °C was tested for the removal of single and binary dyes [28], and Dol heated to 300, 700, and 900 °C was tested for the removal of an anionic dye, methyl orange (MO) [29]. Because of the strong affinity of ARS for calcium and phosphorus, $CaCO_3$ and H_3PO_5 were utilized to synthesize calcium phosphate hydroxyapatite (Ca-Hap), which was tested for its removal of ARS under different physical and chemical conditions [30]. The removal of the anionic dye acid black 210 by Cal reached a capacity of 210 mg/g [31]. Although the removal of yellow 84 azo

dye, also an anionic dye, by amorphous Cal reached a capacity of 40 mg/g [32], the XRD data in the report showed crystallinity of Cal instead of amorphous Cal.

No report, however, could be found for the removal of ARS dye by heat-treated calcite. This knowledge gap represents the primary driving force for this study. Briefly, the removal of ARS by heated Cal was quantified under different physical and chemical conditions. The raw Cal was tested under the same conditions to compare the effectiveness of heat treatment. The interactions between ARS and Cal or HCal were interpreted from the results of experiments and instrumental analyses, and the interaction mechanism was proposed.

2. Materials and Methods

2.1. Materials

The calcite (Cal) was obtained from the mineral collections of the Geosciences Department, University of Wisconsin–Parkside. XRD analyses were conducted first to confirm its purity. The sample was crushed and then ground to less than 0.06 mm. This was the raw calcite serving as the control for comparison. For heat treatment, the ground Cal was placed into a ceramic crucible and heated to 1000 °C for 3 h in a muffle furnace. The heat-treated (HCal) samples were allowed to cool down to room temperature (23 °C) in the oven.

The ARS dye has an IUPAC name of sodium, 3,4-dihydroxy-9,10-dioxo-9,10-dihydroanthracene-2-sulfonate, a formula of $C_{14}H_7NaO_7S$, a molecular mass of 342.253 g/mol, and a CAS# of 130-22-3. Its pKa values are listed as 5.49 and 10.85 [9] with Na^+ as the counterion. Figure 1 shows its speciation under different pH values. Its solubility in water is up to 1 g/L [33]. And its melting point is 287–298 °C [34].
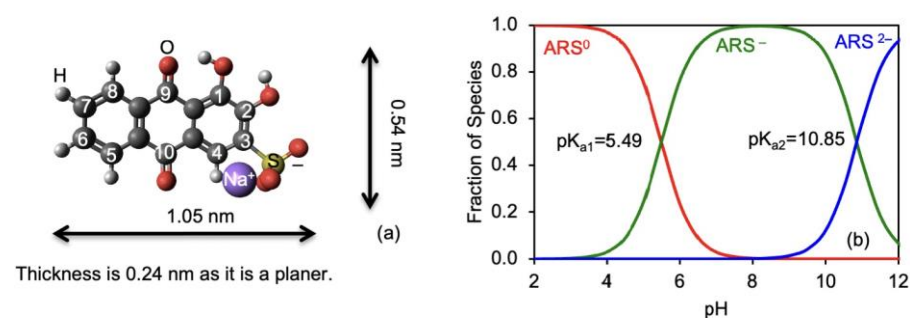

Figure 1. Molecular structure of ARS (**a**) and its pH–speciation diagrams (**b**).

2.2. Batch Sorption Studies for ARS Removal

For all studies, the solid used was either 0.25 or 0.5 g, and the solution used was 10 mL. For the isotherm study, the initial ARS concentrations were up to 2.5 mM for Cal and up to 10 mM for HCal. The equilibrium ionic strength was adjusted to 0.001, 0.01, 0.1, and 1.0 M NaCl for the ionic strength study. For the pH study, concentrated HCl or NaOH were added periodically to adjust the equilibrium pH to 4–12. For the temperature study, 23, 33, 43, and 53 °C were maintained during shaking. The initial ARS concentrations were 0.5 and 6.0 mM for Cal and HCal for the pH and ionic strength studies and 1.0 and 6.0 mM for the temperature and kinetic studies. The samples were mixed for 24 h at 150 rpm on a mechanical shaker. For the kinetic study, samples were shaken for varying amounts of time from ¼ to 24 h. After shaking, all samples were centrifuged at 3500 rpm for 15 min, followed by filtering the supernatants with 0.45 μm syringe filters. The equilibrium ARS concentrations in the supernatants were determined by a UV-Vis method at a wavelength of 420 nm with proper dilution so that the final absorbance values were less than 1.000. The amount of dye sorbed on solid was calculated by the following: C_s (mmol/kg) = ($C_{initial} - C_{equilibrium}$)*volume of liquids (mL)/mass of solid (g).

2.3. Instrumental Analyses

The wavelength used for the ARS measurement was 420 nm. Calibrations were made using ARS concentrations between 0.00 and 0.10 mM. For the pH and ionic studies, the

standards were made at pH 5, 7, 9, and 11 or at ionic strengths of 0.01, 0.1, and 1.0 M NaCl. The solid samples after dye sorption were air-dried naturally and analyzed by XRD and Fourier-transform infrared (FTIR) to determine whether changes in structure or bonding occurred after dye sorption.

A Shimadzu 6100 X-Ray Diffractometer (Columbia, MD, USA) was used for XRD analyses. CuKα radiation at 30 kV and 40 mA with a Ni filter was used. Samples were scanned at 20–60° (2θ) with a speed of 2°/min. A Shimadzu IRXross FTIR spectrometer with a quartz ATR was used for FTIR analyses of the samples after dye sorption. The scan was performed from 400 to 4000 cm^{-1} with a resolution of 2 cm^{-1}. A Shimadzu TGA-50 Analyzer was used for the thermogravimetric measurements. Samples were weighed into platinum crucibles and heated at 20 °C/min to 900 °C.

The SEM observation was performed using a Hitachi S-4800 scanning electron microscope. Samples were loaded onto 13 mm aluminum stubs and then coated with carbon using a vacuum coater (Edwards 306A Coating System). SEM images were taken using 10.0 kV accelerating voltage at a 15.0 mm working distance. The selected elements of each sample were scanned by energy-dispersive X-ray spectroscopy (EDS) (Bruker Quantax Esprit System).

3. Results

3.1. Isotherms of ARS Removal

Under different initial ARS concentrations, the amounts of ARS removed by Cal and HCal varied significantly. As such, ARS removal was plotted against equilibrium ARS concentrations (Figure 2), and data were fitted to several isotherm models. The Langmuir model is as follows:

$$C_s = \frac{K_L S_m C_L}{1 + K_L C_L} \tag{1}$$

where C_L and C_S are the ARS concentration in solution (mmol/L) and sorbed on the solid (mmol/kg). The sorption capacity is S_m (mmol/kg), while the affinity of the ARS for the solid is K_L (L/mmol). A linear form of Equation (1) is as follows:

$$\frac{C_L}{C_s} = \frac{1}{K_L S_m} + \frac{C_L}{S_m} \tag{2}$$
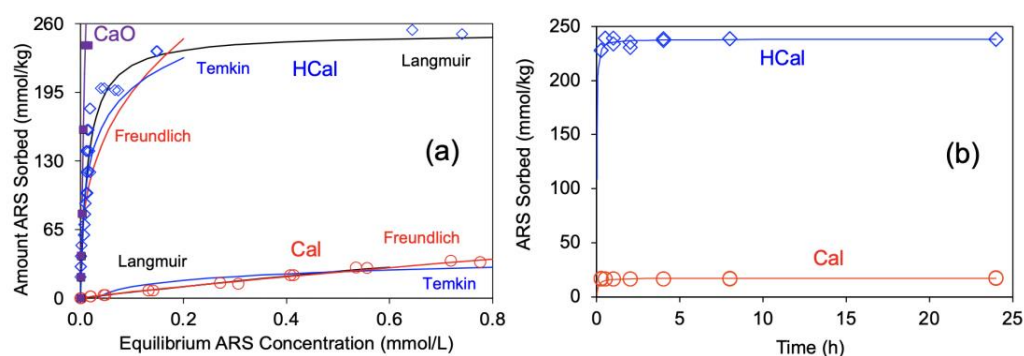

Figure 2. Sorption isotherms (**a**) and kinetics (**b**) of ARS on raw Cal (red circle) and HCal (blue diamond). The Langmuir, Freundlich, and Temkin fitting are indicated by black, red, and blue lines in (**a**). The ARS sorption on CaO is fitted to the Langmuir isotherm only (purple line).

As such, the parameters S_m and K_L can be determined via a linear regression. The fitted parameters are 167 and 251 mmol/kg in S_m and 0.36 and 72 L/mmol in K_L for ARS sorption on Cal and HCal, respectively. The significant difference in K_L values suggests that to achieve a low equilibrium ARS concentration, say 0.05 mM, the amounts of ARS

removed would be 3 mmol/kg and 200 mmol/kg by Cal and HCal. This is about a 70 times increase in ARS removal. The Freundlich isotherm model has the following formula:

$$C_S = K_F C_L^{1/n} \tag{3}$$

It can be rearranged into a linear form:

$$Log C_S = \frac{1}{n} log C_L + log K_F \tag{4}$$

where K_F is the Freundlich isotherm constant and $1/n$ is the intensity of sorption. The K_F values are 45 and 420, while the $1/n$ values are 0.9 and 0.3 for ARS removal by Cal and HCal, suggesting a favorable ARS removal by HCal. The sorption is favorable when $1/n$ is $0 < 1/n < 1$ and unfavorable when $1/n$ is greater than 1 [35]. As such, ARS removal was favored by both Cal and HCal. For ARS sorption on bentonite, the Freundlich isotherm resulted in an r^2 of 0.994 vs. r^2 of 0.74 for the Langmuir sorption isotherm model [24].

The Temkin isotherm is expressed as

$$C_S = \frac{RT}{B_T} \ln(K_T C_L) \tag{5}$$

and it can be rearranged into a linear form:

$$C_S = \frac{RT}{B_T} ln C_L + \frac{RT}{B_T} ln K_T \tag{6}$$

where R is the gas constant, T is the temperature in K, B_T is the Temkin constant related to the heat of sorption (kJ/mol), and K_T is the equilibrium binding constant (L/mol) [36]. The calculated B_T and K_T values are 278 and 60 kJ/mol and 3.5 and 7.1 L/mmol for ARS removal by Cal and HCal, respectively. All fitted parameters based on the three isotherm models are listed in Table 1. For comparison, the sorption of ARS on CaO, which was purchased from Fisher, is also shown in Figure 2, and the observed data were fitted to the Langmuir isotherm model, as it was speculated that CaO was produced after Cal was heated.

Table 1. Parameters of ARS uptake on Cal and HCal from isotherm and kinetic studies.

Sorption Parameters	ARS Sorption on Cal	ARS Sorption on HCal
S_m (mmol/kg)	167	251
K_L (L/mmol)	0.36	72
r^2 for Langmuir isotherm fitting	0.46	0.92
K_F (L/kg)	45	420
$1/n$	0.9	0.3
r^2 for Freundlich isotherm fitting	0.99	0.91
B_T (kJ/mol)	278	60
K_T (L/mmol)	3.5	7.1
r^2 for Temkin isotherm fitting	0.84	0.87
q_e (mmol/kg)	17	238
kq_e^2 (mmol/kg-h)	213	20,000
k (kg/mmol-h)	0.7	0.35
r^2 for pseudo-second-order fitting	0.9999	0.9999

Most of the studies on ARS removal have focused on using modified or synthetic materials, such as polyethyleneimine-functionalized magnetic carbon nanotubes [37], as most Earth materials are negatively charged on their surfaces and ARS is an anionic dye. Thus, the net repulsive interaction prevented the use of raw Earth materials for ARS removal. Still, the sorptive removal of ARS was evaluated using LDH with an ARS removal of 29 mg/g [25] and using bentonite with a capacity of 170 mg/g [24]. In another study, an activated clay modified by iron oxide achieved an ARS removal capacity of 33 mg/g, but the XRD data showed the dominant mineral was quartz, and no clay mineral was detected [26]. The sorption of ARS on Fe_2O_3-coated biochar/kaolin reached a capacity of 175 mg/g [27]. In the current study, the ARS sorption capacity reached 251 mmol/kg or 86 mg/g on HCal based on the Langmuir isotherm fitting (Figure 2a), showing great promise for using Earth materials, or calcite in this case, for the removal of anionic contaminants after heat treatment.

3.2. Kinetics of ARS removal

Under different contact times, the amount of ARS removed is plotted in Figure 2b. Several kinetic models were utilized to fit the experimental data. The pseudo-second-order kinetic model has the formula

$$q_t = \frac{kq_e^2 \, t}{1+kq_e t} \tag{7}$$

which can be rearranged into a linear form:

$$\frac{t}{q_t} = \frac{1}{kq_e^2} + \frac{1}{q_e}t \tag{8}$$

where k and kq_e^2 are the rate constant and initial rate of ARS removal by the solid with units of kg/mmol/h and mmol/kg/h, and q_t and q_e are the amounts of ARS removal at time t and at equilibrium with a unit of mmol/kg. For ARS removal by Cal from an initial concentration of 1.0 mM, the q_e was 17 mmol/kg, while the k was 0.7 kg/mmol/h. After heat treatment, with an initial concentration of 6.0 mM, the q_e increased to 238 mmol/kg, although the k was decreased by 50% to 0.35 kg/mmol/h. The kq_e^2 values are 213 and 20,000 mmol/kg/h for ARS removal by Cal and HCal (Table 1). For comparison, ARS removal by halloysite showed a q_e value of 33.3 mmol/kg and a kq_e^2 value of 222 mmol/kg/h [5]. Again, the results show significant promise for using Earth materials for anionic contaminant removal after heat treatment.

3.3. Effect of Equilibrium Solution pH, Ionic Strength, and Temperature on ARS Removal

With pKa values of 5.49 and 10.85 [9], ARS could be in neutral form when the solution pH is less than its pKa1 value, monoanionic base when the solution pH is between its pKa1 and pKa2 values, and dianionic base when the solution pH is higher than its pKa2 values (Figure 1). However, the removal of ARS by Cal and HCal is less affected by equilibrium solution pH, varying from 220 to 240 mmol/kg for HCal and 7 to 9 mmol/kg for Cal (Figure 3a). A slight decrease in ARS removal (from 240 to 220 for HCal and 9 to 7 for Cal) was found at pH 12. Similarly, ARS sorption on an activated clay modified by iron oxide decreased slightly from 24.6 mg/g at pH 3 to 23.4 mg/g at pH 11 [26]. ARS sorption on a biosorbent of mustard husk decreased from 100% at pH 2 to 45–50% at pH 9–10 with initial concentrations of 25, 50, and 100 mg/L [38]. Higher pH values promoted the solubility of alizarin (AZ) in aqueous solution, as such, higher pH values negatively influenced AZ sorption on halloysite from 9.8 mg/g at pH 9 to 4.8 mg/g at pH 13 [39]. Similarly, ARS sorption on magnetite–talc composite materials decreased from 75% at pH 2 to 15% at pH 10 [23].
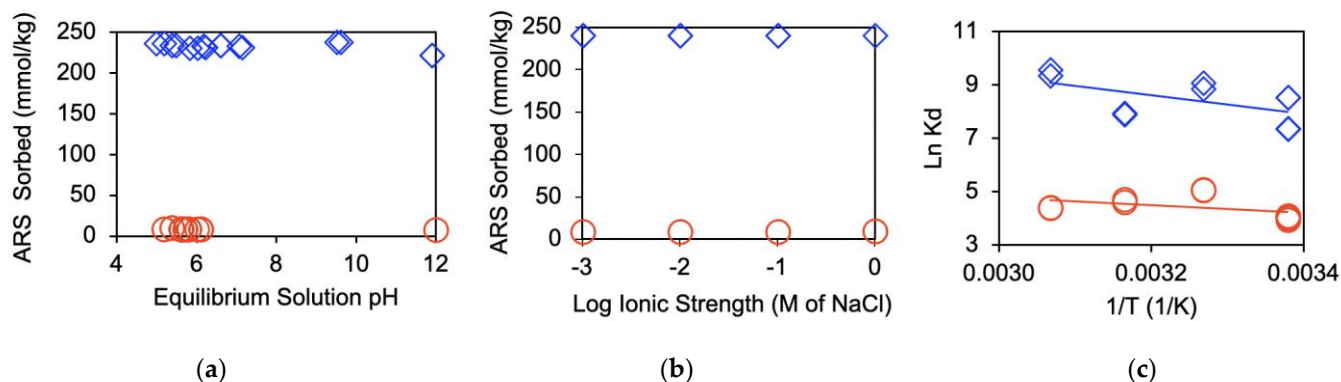
(a)   (b)   (c)

Figure 3. Influence of equilibrium solution pH (**a**), ionic strength (**b**), and temperature (**c**) on ARS sorption on Cal (red circle) and HCal (blue diamond).

The solution ionic strength had a minimal influence on ARS removal by Cal and HCal. The ARS removal was about 240 mmol/kg for HCal in comparison to 9 mmol/kg for Cal, an increase of more than 25 times (Figure 3b). Still, the equilibrium ARS concentrations were less than 0.005 mM with an initial concentration of 6.0 mM when HCal was used, in comparison to equilibrium concentrations of 0.03 to 0.08 mM with an initial ARS concentration of 0.5 mM when Cal was used.

ARS sorption as affected by equilibrium temperature is depicted in Figure 3c. The thermodynamics for solute sorption from solution is governed by

$$\ln K_d = -\frac{\Delta H}{RT} + \frac{\Delta S}{R} \tag{9}$$

where K_d is the distribution coefficient of the solute, ΔH and ΔS are the changes in enthalpy and entropy after solute sorption on solid surfaces, and R and T are gas constant and temperature in K. The ΔG is the change in free energy after solute sorption and is related to ΔH and ΔS by

$$\Delta G = \Delta H - T\Delta S \tag{10}$$

The ΔH values are 12 and 29 kJ/mol, the ΔS values are 0.06 and 0.16 kJ/mol/K, and the ΔG values are -10 to -13 and -20 to -25 kJ/mol for ARS sorption on Cal and HCal, respectively, suggesting a spontaneous and endothermic sorption, resulting in an increase in disorder of the sorbed ARS molecules on the surface, and the interactions between the ARS molecules and the surfaces of Cal and HCal are relatively weak, such as electrostatic interactions.

3.4. XRD Analyses

The XRD patterns of Cal and HCal after ARS sorption are presented in Figure 4. For reference purposes, the XRD pattern of CaO is also plotted in Figure 4. The literature showed some discrepancies in the locations and assignments of CaO diffraction peaks. In one study, the XRD peaks for CaO were located at 32.10°, 37.50°, and 54.20°, corresponding to (111), (200), and (311), with relative intensities of 30, 100, and 40 [40]. In a different study, the CaO peaks were listed at 18.02°, 34.12°, and 50.85° for the three highest intensities [41]. Another study showed peaks located at 32.5°, 36.6°, 38.2°, 44.5°, 45.4°, 64.2°, 67.8°, 77.4°, and 81.8° (JCPDS card No. 00-004-0777) [42]. The XRD peaks of CaO were at 29.59°, 32.22°, 37.35°, 42.81°, 53.83°, 64.09°, and 67.34°, corresponding to diffractions of (011), (111), (002), (012), (022), (113), and (222), agreeing with CaO (lime, syn, JCPDS card No. 00-004-0777) with a cubic crystal system and lattice parameters (5.8152 Å) [43]. In this study, they are located at 32.20°, 37.34°, and 53.86°, agreeing with those of Kumar et al. [40] (Figure 4). These peaks were not found in the HCal samples after being in contact with different ARS solutions for 24 h, suggesting that either CaO is not present in the system or is converted back into calcite after being in contact with ARS solutions for 24 h and then being air-dried.
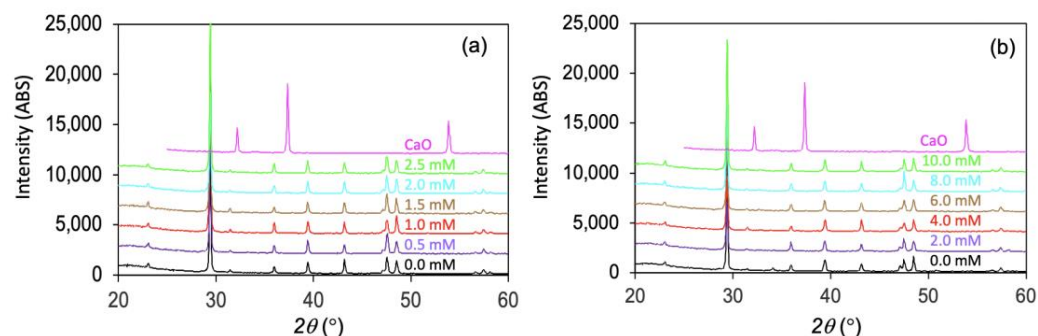
Figure 4. XRD patterns of Cal (**a**) and HCal (**b**) after ARS sorption at different concentrations.

From the XRD analyses of Cal and HCal, the following observation could be identified. Firstly, the *d*-spacing of Cal remained the same after it was heated to 1000 °C for 3 h. The (111) peak of CaO at 32.34° 2θ and the (101) peak of $Ca(OH)_2$ at 34.11° 2θ [44] are not present in the XRD patterns of HCal either, suggesting that neither was produced after being heated at 1000 °C for 3 h or converted back into calcite after being shaken for 24 h in ARS solution. Meanwhile, an early study on the XRD patterns of ARS showed peaks at 26.38, 31.72, and 45.44° 2θ due to the reflections of (−304), (222), and (−434) [45]. Secondly, no diffraction peaks of CaO or ARS were found in these samples, suggesting that the mineral phase was not altered (remained as calcite) after heat treatment, and no crystalline ARS was found on Cal or HCal surfaces. Thirdly, the *d*-spacing of calcite did not change after ARS sorption, indicating that the sorption sites were on the external surfaces.

3.5. FTIR Analyses

For nano-CaO, the bands located at 3642 cm^{-1} are assigned to the O–H free hydroxyl bond from the residual hydroxide or the moisture content in the sample, the ones at 1471 cm^{-1} and 876 cm^{-1} indicate the C–O bond due to the carbonation of CaO nanoparticles, and the two small dips at 1229 cm^{-1} and 1633 cm^{-1} and the band at 2515 cm^{-1} are attributed to C–O stretch of the CO_2 stretching [40]. In this study, these bands are very weak, suggesting that the CaO had low crystallinity.

For crystalline ARS, the bands are at 3448 cm^{-1} for ν(OH) due to hydrogen bonding, at 1634 cm^{-1} for ν (10-C=O), at 1589 cm^{-1} for ν (9-C=O), at 1546 cm^{-1} and 1499 cm^{-1} for ν (Ar C=C), at 1191 cm^{-1} for ν (C–O), at 1069 cm^{-1} for $\nu_{as}(SO_3)$, at 1037 cm^{-1} for $\nu_s(SO_3)$, and at 1127 cm^{-1} for carbonyl C–C–C [46]. None of these bands showed up on the FTIR spectra of Cal and HCal after ARS sorption (Figure 5). This could be due to the lower amounts of ARS on Cal or HCal surfaces.
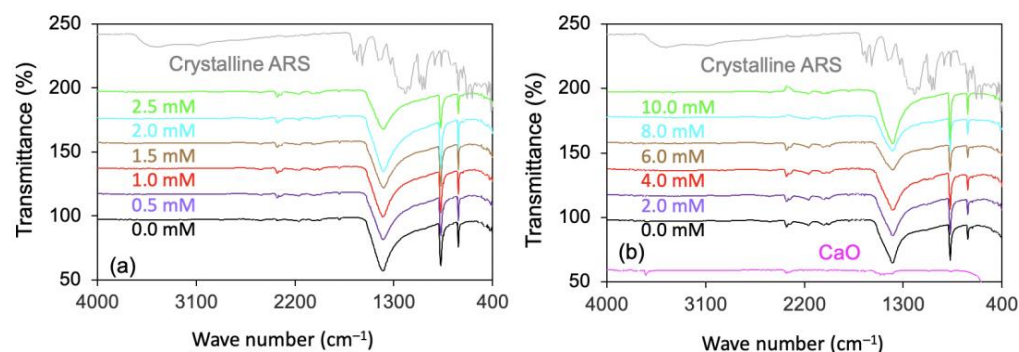

Figure 5. FTIR spectra of Cal (**a**) and HCal (**b**) after ARS sorption at different initial concentrations. The transmittance is in arbitrary value units due to overlay of the FTIR spectra vertically.

For Cal, the sharp intense band at 873 cm^{-1} was assigned to the O–C stretching of $CaCO_3$, and the band at 713 cm^{-1} is due to the OCO bending [47]. In this study, for the Cal samples, they were located at 872 and 712 cm^{-1} and stayed the same regardless of the

amount of ARS sorption (Figure 5). However, for the HCal samples, they were located at 872 and 712 cm^{-1} when the ARS loading level was low and shifted to 874 and 727 cm^{-1} when the ARS loading was high (Figure 5). This may suggest slight changes in binding between ARS and HCal from low to high ARS sorption levels.

3.6. SEM Observation and ETF Scans

The SEM observation showed no changes in the particle morphology and particle size between Cal and HCal (Figure 6). In addition, the {104} cleavage is still visible and very well developed after Cal was heated to 1000 °C for 3 h (Figure 6b), confirming the XRD analyses. The element scan for S and Na was also conducted to see the sorption of ARS and the counterion Na$^+$. A significant increase in the S density was noticed for HCal after ARS sorption (Figure 6d), in comparison to the S density on Cal after ARS sorption (Figure 6c). In contrast, the Na density was about the same for Cal and HCal after ARS sorption (Figure 6e,f), suggesting that the enhanced ARS sorption on HCal was not associated with counterion Na$^+$ sorption.
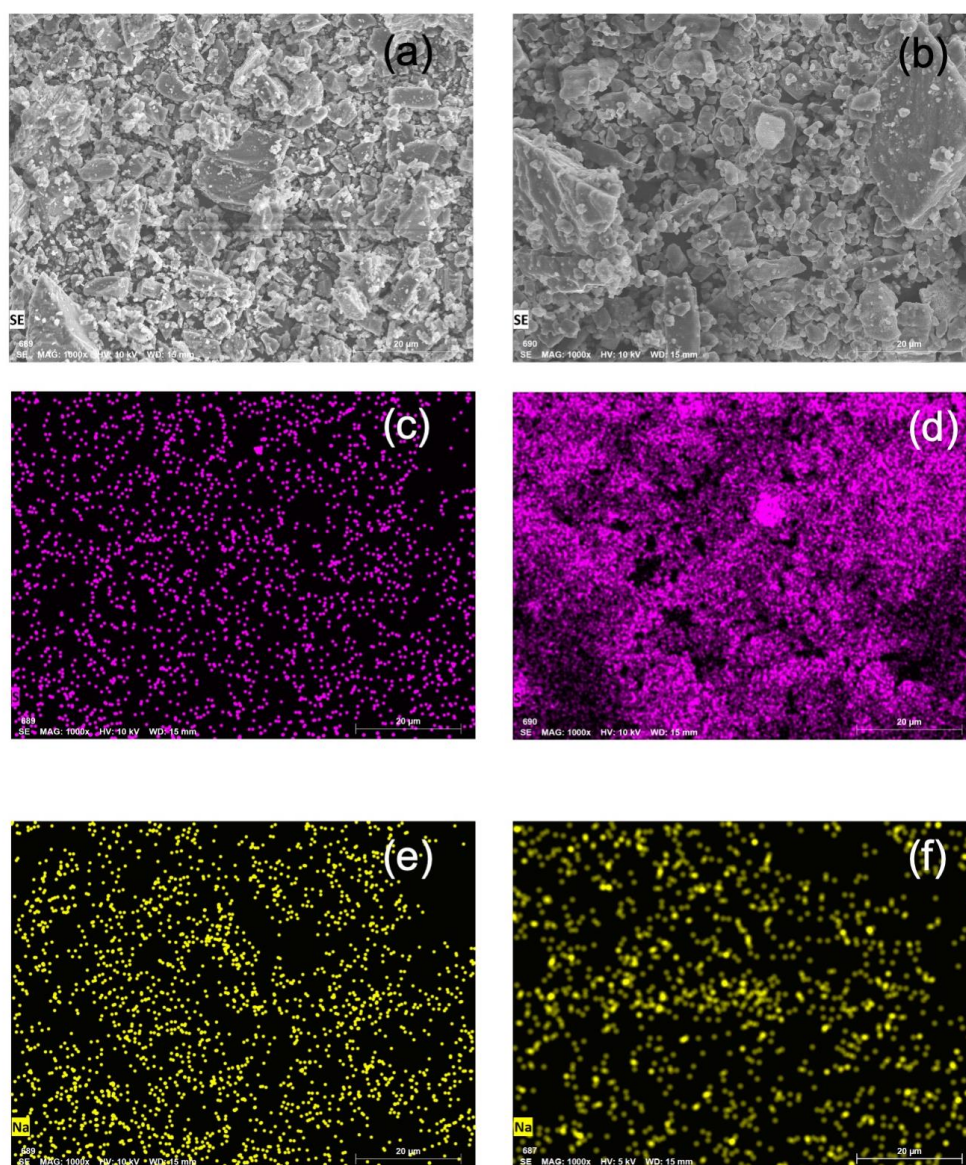

Figure 6. SEM images of Cal (**a**) and HCal (**b**), the ETF scan of S on Cal (**c**) and HCal (**d**), and the ETF scan of Na on Cal (**e**) and HCal (**f**).

3.7. TGA Analyses

The TGA analyses of the Cal and HCal can be seen in Figure 7. For Cal, the decomposition started at 710 °C and ended at 790 °C with a weight loss of 43%, agreeing well with standard calcite TGA data [48]. In contrast, the major decomposition for HCal started at 420 °C and ended at 460 °C. This could be due to the breakdown of $Ca(OH)_2$. In a study of TGA analyses of CaO exposed to ambient moisture for several days, $Ca(OH)_2$ decomposition between 350 and 400 °C was found [49]. However, in this study, it is almost identical to that of CaO (Figure 7a).

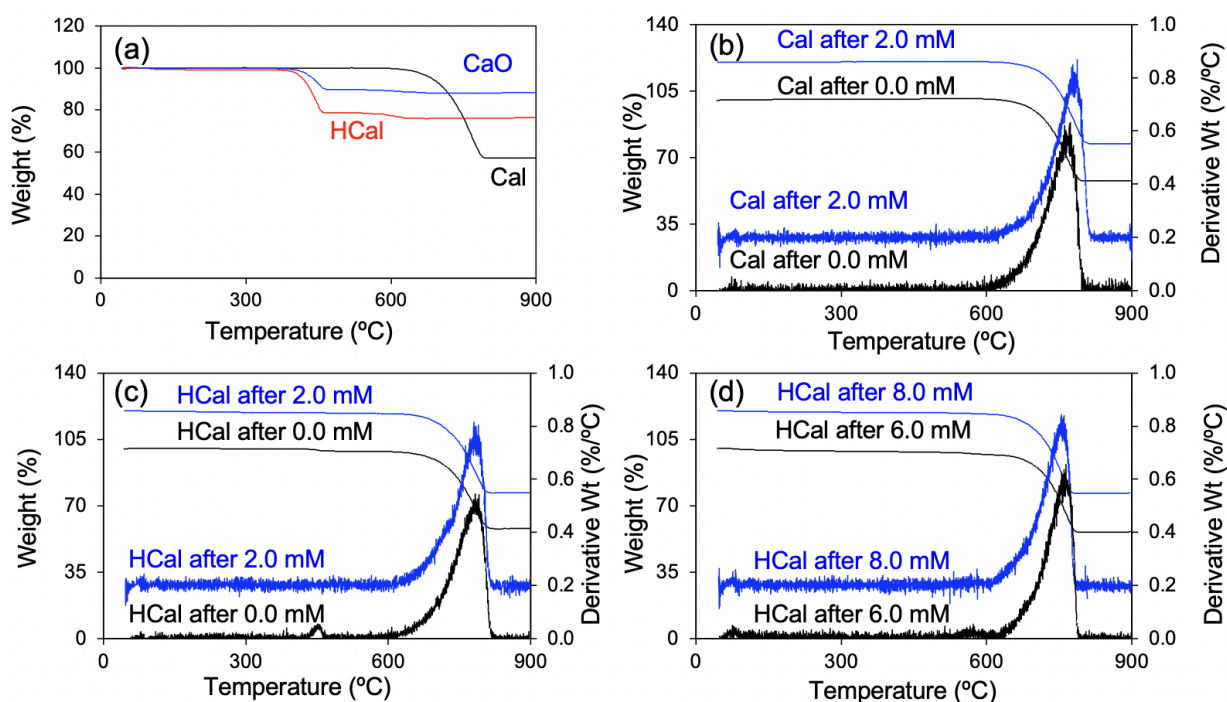**Figure 7.** TGA and DTG analyses of Cal, HCal, and CaO (**a**), Cal (**b**) and HCal (**c,d**) at different initial concentrations. The left y-axis is for TGA, and the right y-axis is for DTG. The blue lines in (**b–d**) are a 20% upshift of the left y-axis and a 0.2%/°C upshift of the right y-axis.

The second decomposition started at 600 °C and ended at 630 °C. This could be due to the breakdown of calcite. Thus, the TGA results showed a significant difference between Cal and HCal. This could be caused by the fact that the HCal was air-dried in the oven and was never in contact with water, and the minute amount of calcite production could be due to the reaction of CaO with moisture and CO_2 in the air during the storage process.

For Cal after sorption with ARS, the TGA results matched well with the raw Cal (Figure 7b). However, for the HCal after equilibration with different initial concentrations of ARS, the TGA data showed different patterns to those of HCal, i.e., the decomposition temperature corresponding to CaO disappeared (Figure 7c,d), but were almost identical to the TGA of Cal, suggesting that after being in contact with water or ARS solution for 24 h and then being dried in the air, there is a significant conversion back from CaO to calcite. It was previously reported that after Cal was heated to 900 °C, CaO was produced, and in the presence of moisture, the CaO would convert to $Ca(OH)_2$ [50]. This study suggested that CaO produced after Cal decomposition at 900 °C could be converted back into calcite.

4. Discussion

The interaction of Ca^{2+} with ARS was used for Ca stain [16]. Thus, due to the presence of Ca^{2+} on the Cal surfaces, it was anticipated that Cal would be able to sorb a significant amount of ARS. However, the preliminary study using 0.1 and 0.2 mM ARS for its sorption on Cal and HCal heated to 600 and 800 °C resulted in similar sorption (about 70%) removal.

To achieve higher ARS removal, Cal was heated to 1000 °C in this study. The ARS removal capacities are 167 and 251 mmol/kg, but the affinity values of ARS for Cal and HCal are 0.36 and 72 L/mmol. The significant difference in K_L values suggests that HCal is extremely effective in the removal of ARS at low initial concentrations. To achieve an equilibrium ARS concentration of 0.05 mM, the amounts of ARS removed would be 3 mmol/kg or 200 mmol/kg when Cal or HCal were used.

The solution pH played an important role in ARS sorption onto the {104} cleavage of Cal. At a low pH, only one hydroxyl group is deprotonated, resulting in a possible adsorption configuration mediated by the 3-C–O$^-$ and 4-C–OH groups [51]. When the pH is above 8, both hydroxyl groups are deprotonated, and the ARS molecules bind to two C–O$^-$ groups on the surface of Cal. However, the solution pH had a minimal effect on ARS removal in this study, suggesting that the {104} cleavage may not play an important role as the ARS sorption surface.

A previous study showed that Ca can react with ARS via its sulfonic acid and/or its OH groups [16]. Under different solution pH, the relative amount of the three ARS species would be different. With an increase in the pH, electrochemical reduction may lead to the dissociation of four phenolic hydroxyl groups, resulting in the formation of seven different species, with negative charges located on different O [52]. In addition, the binding between Ca^{2+} and ARS could be of salt type, by which the Ca^{2+} complexes with O atoms attached to C1 and C2, or of chelate type, by which the Ca^{2+} complexes with O atoms attached to C1 and C9 [9]. For the former case, the binding between Ca^{2+} and ARS could be 1:1, or 1:2 in a dimeric formation (Figure 8). These were just speculations based on the amount of ARS sorbed on Cal and HCal.
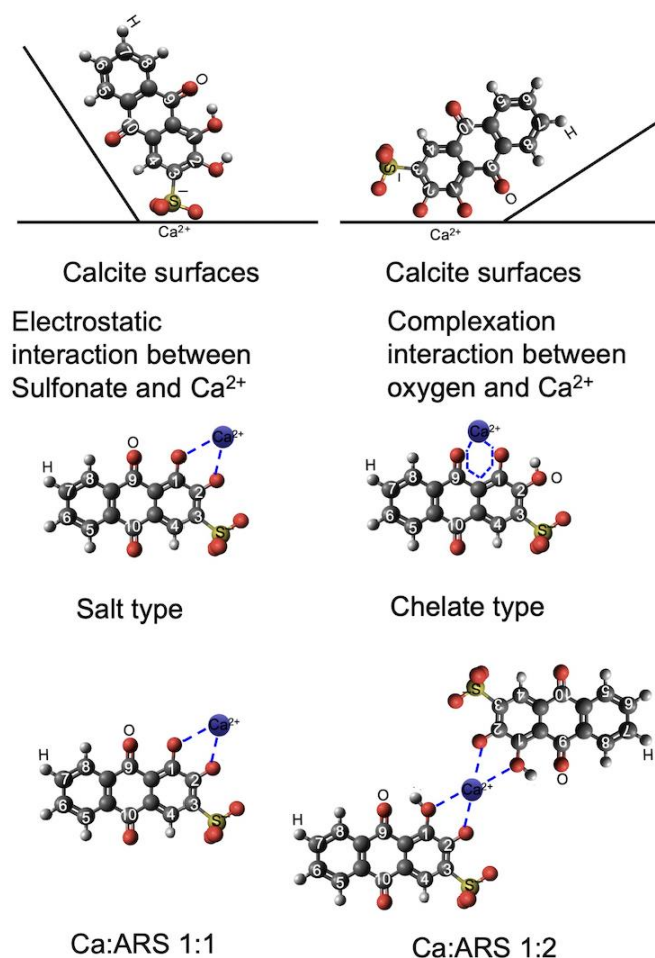

Figure 8. Illustration of electrostatic interaction (**left**) or complexation interaction (**right**) of ARS on Cal or HCal surfaces.

As the reaction between ARS and Ca^{2+} was widely used for Ca stain [35], it was anticipated that calcite would be able to sorb ARS due to the presence of Ca^{2+} on the surface. However, the ARS sorption on Cal was much lower in comparison to HCal. In a previous study, when ARS sorbed on HDol surfaces, it was speculated that salt-type or chelate-type interactions between Ca^{2+} and ARS were responsible for the enhanced ARS removal by HDol [53]. In this study, the same type of interactions may also contribute to the much-enhanced ARS removal by HCal. On the other hand, as the XRD pattern of HCal before being added to water showed dominant CaO peaks, the significant increase in ARS removal by HCal could be due to the interactions between ARS and Ca^{2+} from CaO, which could be converted back to calcite in aqueous media. This mechanism would also explain why the mineral phase was still calcite for HCal samples after ARS sorption (Figures 4 and 5). Previous results showed that the ARS sorption capacity on CaO was up to 1 mg/g [54]. In this study, the ARS sorption capacity was 251 mmol/kg, or 86 mg/g. This is significantly higher than in the previous study [54]. As such, the heat treatment of calcite not only increased the ARS removal in comparison to Cal but also in comparison to CaO, which is reported for the first time in this study.

5. Conclusions

In this study, the removal of color dye ARS by calcite after heat treatment was evaluated in detail under different physico-chemical conditions. The ARS removal capacity increased from 167 mmol/kg to 251 mmol/kg, a 50% increase, following the heat treatment of calcite. Additionally, the Langmuir coefficient increased from 0.36 to 72 L/mmol, an increase of 200 times. Such an increase would make HCal much more effective in removing ARS. The removal of ARS by HCal could be attributed to the formation of complexation with Ca^{2+} on the solid surface. Thus, the heat treatment of calcite in this study indicated a new approach and the effective utilization of Earth materials such as limestone for the removal of industrial contaminants from water in addition to their general use as raw materials for manufacturing cement and as construction materials.

Author Contributions: Conceptualization, Z.L. and S.X.; methodology, L.A., Z.L. and S.X.; investigation, A.R., A.B. and J.S.; resources, Z.L.; data curation, A.R., A.B. and J.S.; writing—original draft preparation, Z.L.; writing—review and editing, Z.L.; visualization, Z.L.; supervision, Z.L.; project administration, Z.L.; funding acquisition, Z.L. All authors have read and agreed to the published version of the manuscript.

Data Availability Statement: Due to patent application, the data pertaining to the original contributions presented in this study are stored at the University of Wisconsin–Parkside. Further inquiries can be directed to the corresponding author.

Conflicts of Interest: The authors declare no conflicts of interest.

References

1. Abuessawy, A.A.; Fouda, A.F.; Adel, A.H.; Hawata, M.A.H.; Hamad, N.A.H. New modified heterocyclic-magnetite chitosan nanocomposite for efficient alizarin red dye removal: Adsorption analysis and antibacterial activity. *J. Polymer. Environ.* **2024**, *32*, 826–841. [CrossRef]
2. Katheresan, V.; Kansedo, J.; Lau, S.Y. Efficiency of various recent wastewater dye removal methods: A review. *J. Environ. Chem. Engineer.* **2018**, *6*, 4676–4697. [CrossRef]
3. Ngulube, T.; Gumbo, J.R.; Masindi, V.; Maity, A. An update on synthetic dyes adsorption onto clay based minerals: A state-of-art review. *J. Environ. Manag.* **2017**, *191*, 35–57. [CrossRef] [PubMed]
4. Wang, X.; Baker, J.; Carlson, K.; Li, Z. Mechanisms of selected anionic dye removal by clinoptilolite. *Crystals* **2022**, *12*, 727. [CrossRef]

5.　Shi, Y.; Baker, J.; Feng, C.; Wang, X.; Li, Z. Removal of toluidine blue from water using 1: 1 layered clay minerals. *Adv. Powder Technol.* **2022**, *33*, 103608. [CrossRef]

6.　Largo, F.; Haounati, R.; Akhouairi, S.; Ouachtak, H.; El Haouti, R.; El Guerdaoui, A.; Hafid, N.; Santos, D.M.; Akbal, F.; Kuleyin, A.; et al. Adsorptive removal of both cationic and anionic dyes by using sepiolite clay mineral as adsorbent: Experimental and molecular dynamic simulation studies. *J. Molec. Liq.* **2020**, *318*, 114247. [CrossRef]

7.　Rao, W.; Piliouras, P.; Wang, W.; Guido, A.; Kugler, K.; Sieren, B.; Wang, L.; Lv, G.; Li, Z. Zwitterionic dye rhodamine B (RhB) uptake on different types of clay minerals. *Appl. Clay Sci.* **2020**, *197*, 105790. [CrossRef]

8.　Rodrigues, I.A.; Villalba, J.C.; Santos, M.J.; Melquiades, F.L.; Anaissi, F.J. Smectitic clays enriched with ferric ions for the rapid removal of anionic dyes in aqueous media. *Clay Miner.* **2020**, *55*, 12–23. [CrossRef]

9.　Lemlikchi, W.; Sharrock, P.; Fiallo, M.; Nzihou, A.; Mecherri, M.O. Hydroxyapatite and Alizarin sulfonate ARS modeling interactions for textile dyes removal from wastewaters. *Procedia Engineer.* **2014**, *83*, 378–385. [CrossRef]

10.　Friedman, G.M. Identification of carbonate minerals by staining methods. *J. Sediment. Res.* **1959**, *29*, 87–97.

11.　Dickson, J.A.D. Carbonate identification and genesis as revealed by staining. *J. Sediment. Res.* **1966**, *36*, 491–505.

12.　Fu, E.; Somasundaran, P. Alizarin Red S as a flotation modifying agent in calcite-apatite systems. *Int. J. Miner. Process.* **1986**, *18*, 287–296. [CrossRef]

13.　King, H.G.C.; Pruden, G. The purification of commercial Alizarin Red S for the determination of aluminium in silicate minerals. *Analyst* **1968**, *93*, 601–605. [CrossRef]

14.　Wang, X.; Wang, Y.; Zhu, X.; Wang, X.; Zhang, Q.; Lu, Y.; Wang, X.; Yang, X. Method for Determination of Aluminum Ion Content by Alizarin Red S Complexation Spectrophotometry; 2014. Available online: https://patents.google.com/patent/CN103994980A/en (accessed on 28 April 2024).

15.　Parker, C.A.; Goddard, A.P. The reaction of aluminium ions with alizarin-3-sulphonate with particular reference to the effect of addition of calcium ions. *Anal. Chim. Acta* **1950**, *4*, 517–535. [CrossRef]

16.　Puchtler, H.; Meloan, S.N.; Terry, M.S. On the history and mechanism of alizarin and alizarin red S stains for calcium. *J. Histochem. Cytochem.* **1969**, *17*, 110–124. [CrossRef]

17.　CGregory, A.; Gunn, W.G.; Peister, A.; Prockop, D.J. An Alizarin red-based assay of mineralization by adherent cells in culture: Comparison with cetylpyridinium chloride extraction. *Anal. Biochem.* **2004**, *329*, 77–84. [CrossRef] [PubMed]

18.　Wu, L.; Forsling, W. Potentiometric and spectrophotometric study of calcium and alizarin S complexation. *Acta Chem. Scand.* **1992**, *46*, 418–422. [CrossRef]

19.　Wu, L.; Forsling, W. Holmgren, Surface complexation of calcium minerals in aqueous solution. 4. The Complexation of Alizarin Red S at Fluorite–Water Interfaces. *J. Colloid Interface Sci.* **2020**, *224*, 211–218. [CrossRef] [PubMed]

20.　Rehman, R.; Mahmud, T.; Anwar, J.; Salman, M.; Shafique, U.; Zaman, W.U.; Ali, F. Removal of alizarin red s (dye) from aqueous media by using alumina as an adsorbent. *J. Chem. Soc. Pak* **2011**, *33*, 228–232.

21.　Ghaedi, M.; Najibi, A.; Hossainian, H.; Shokrollahi, A.; Soylak, M. Kinetic and equilibrium study of Alizarin Red S removal by activated carbon. *Toxicol. Environ. Chem.* **2012**, *94*, 40–48. [CrossRef]

22.　Narayan, R.T.; Ashwini, A.; Veeranna, K.D. Removal of alizarin red dye using calcium hydroxide as a low-cost adsorbent. *J. Appl. Chem. Res.* **2016**, *10*, 35–47.

23.　Nayl, A.A.; Abd-Elhamid, A.I.; Ahmed, I.M.; Bräse, S. Preparation and characterization of magnetite talc (Fe$_3$O$_4$@ Talc) nanocomposite as an effective adsorbent for Cr (VI) and alizarin red S dye. *Materials* **2022**, *15*, 3401. [CrossRef] [PubMed]

24.　EEl-Menofy, A.; Ali, O.I.; Kandil, A.H.T. Removal of alizarin red s from aqueous solution using sodium bentonite. *Arab. Univ. J. Agric. Sci.* **2018**, *26*, 1967–1974. [CrossRef]

25.　Al-Salihi, K.J.; Alfatlawi, W.R. Synthesis and characterization of low-cost adsorbent and used for Alizarin yellow GG and alizarin Red S dyes removal from aqueous solutions. In *IOP Conference Series: Materials Science and Engineering, Volume 1094, 1st International Conference on Sustainable Engineering and Technology (INTCSET 2020), Baghdad, Iraq, 15–16 December 2020*; IOP Publishing: Bristol, UK, 2021.

26.　Fu, F.; Gao, Z.; Gao, L.; Li, D. Effective adsorption of anionic dye, alizarin red S, from aqueous solutions on activated clay modified by iron oxide. *Industr. Engineer. Chem. Res.* **2011**, *50*, 9712–9717. [CrossRef]

27.　Ohale, P.E.; Chukwudi, K.; Ndive, J.N.; Michael, M.E.; Abonyi, M.N.; Chukwu, M.M.; Obi, C.C.; Onu, C.E.; Igwegbe, C.A.; Azie, C.O. Optimization of Fe$_2$O$_3$@ BC-KC composite preparation for adsorption of Alizarin red S dye: Characterization, kinetics, equilibrium, and thermodynamic studies. *Results Surf. Interfaces* **2023**, *13*, 100157. [CrossRef]

28.　Shirazi, E.K.; Metzger, J.W.; Fischer, K.; Hassani, A.H. Simultaneous removal of a cationic and an anionic textile dye from water by a mixed sorbent of vermicompost and Persian charred dolomite. *Chemosphere* **2019**, *234*, 618–629. [CrossRef] [PubMed]

29.　Zahuri, A.A.; Patah, M.F.A.; Kamarulzaman, Y.; Hashim, N.H.; Thirumoorthi, T.; Mohtar, W.H.M.W.; Hanafiah, Z.M.; Amir, Z.; Wan-Mohtar, W.A.A.Q.I. Decolourisation of real industrial and synthetic textile dye wastewater using activated dolomite. *Water* **2023**, *15*, 1172. [CrossRef]

30.　Adeogun, A.I.; Babu, R.B. One-step synthesized calcium phosphate-based material for the removal of alizarin S dye from aqueous solutions: Isothermal, kinetics, and thermodynamics studies. *Appl. Nanosci.* **2021**, *11*, 1–13. [CrossRef]

31.　Talhi, A.; Merabet, S.; Bouhouf, L.; Boukhalfa, C. *Removal of Acid black* 210 by adsorption on calcite. *Desal. Water Treat.* **2020**, *205*, 407–411. [CrossRef]

32. Brinza, L.; Maftei, A.E.; Tascu, S.; Brinza, F.; Neamtu, M. Advanced removal of Reactive Yellow 84 azo dye using functionalised amorphous calcium carbonates as adsorbent. *Sci. Rep.* **2022**, *12*, 3112. [CrossRef]

33. Available online: https://www.chemicalbook.com/ChemicalProductProperty_EN_CB0711917.htm (accessed on 7 April 2024).

34. Available online: https://www.scbt.com/p/alizarin-red-s-130-22-3 (accessed on 7 April 2024).

35. Al-Ghouti, M.A.; Da, D.A. Guidelines for the use and interpretation of adsorption isotherm models: A review. *J. Hazard. Mater.* **2020**, *393*, 122383. [CrossRef] [PubMed]

36. Zhou, X.; Maimaitiniyazi, R.; Wang, Y. Some consideration triggered by misquotation of Temkin model and the derivation of its correct form. *Arab. J. Chem.* **2022**, *15*, 104267. [CrossRef]

37. Zhang, Z.; Chen, H.; Wu, W.; Pang, W.; Yan, G. Efficient removal of Alizarin Red S from aqueous solution by polyethyleneimine functionalized magnetic carbon nanotubes. *Bioresour. Technol.* **2019**, *293*, 122100. [CrossRef] [PubMed]

38. Gautam, R.K.; Banerjee, S.; Gautam, P.K.; Rawat, V.; Kumar, A.; Singh, S.K.; Chattopadhyaya, M.C. Biosorption of an Acidic Dye, Alizarin Red S, Onto biosorbent of mustard husk: Kinetic, equilibrium modeling and spectroscopic analysis. *Asian J. Res. Chem.* **2014**, *7*, 417–425.

39. Zhuang, G.; Rodrigues, F.; Zhang, Z.; Fonseca, M.G.; Walter, P.; Jaber, M. Dressing protective clothing: Stabilizing alizarin/halloysite hybrid pigment and beyond. *Dye. Pigment.* **2019**, *166*, 32–41. [CrossRef]

40. Kumar, S.; Sharma, V.; Pradhan, J.K.; Sharma, S.K.; Singh, P.; Sharma, J.K. Structural, Optical and Antibacterial Response of CaO Nanoparticles Synthesized via Direct Precipitation Technique. *Nano Biomed. Eng.* **2021**, *13*, 172–178. [CrossRef]

41. Ramli, M.; Rossani, R.B.; Nadia, Y.; Darmawan, T.B.; Febriani, S.; Ismail, Y.S. May. Nanoparticle fabrication of calcium oxide (CaO) mediated by the extract of red dragon fruit peels (*Hylocereus polyrhizus*) and its application as inorganic–anti-microorganism materials. *IOP Conf. Ser. Mater. Sci. Engineer.* **2019**, *509*, 012090. [CrossRef]

42. Aghaee, M.; Manteghi, F. Antibacterial Activity of Ag_2O/SrO/CaO Nanocomposite. *Chem. Proceed.* **2022**, *12*, 77.

43. Jadhav, V.; Bhagare, A.; Wahab, S.; Lokhande, D.; Vaidya, C.; Dhayagude, A.; Khalid, M.; Aher, J.; Mezni, A.; Dutta, M. Green synthesized calcium oxide nanoparticles (CaO NPs) using leaves aqueous extract of moringa oleifera and evaluation of their antibacterial activities. *J. Nanomater.* **2022**, *2022*, 9047507. [CrossRef]

44. Blanton, T.N.; Barnes, C.L. Quantitative analysis of calcium oxide desiccant conversion to calcium hydroxide using X-ray diffraction. *Adv. X-ray Anal.* **2005**, *28*, 45–51. [CrossRef]

45. El-Nahass, M.M.; Zeyada, H.M.; El-Ghamaz, N.A. Structural investigation, thermal analysis and AC conduction mechanism of thermally evaporated alizarin red S thin films. *Optik* **2018**, *170*, 304–313. [CrossRef]

46. Chin, Y.P.; Raof, S.F.A.; Sinniah, S.; Lee, V.S.; Mohamad, S.; Manan, N.S.A. Inclusion complex of Alizarin Red S with β-cyclodextrin: Synthesis, spectral, electrochemical and computational studies. *J. Molec. Struct.* **2015**, *1083*, 236–244. [CrossRef]

47. Gupta, U.; Singh, V.K.; Kumar, V.; Khajuria, Y. Experimental and theoretical spectroscopic studies of calcium carbonate ($CaCO_3$). Mater. *Focus* **2015**, *4*, 164–169.

48. Villagrán-Zaccardi, Y.A.; Egüez-Alava, H.; De Buysser, K.; Gruyaert, E.; De Belie, N. Calibrated quantitative thermogravimetric analysis for the determination of portlandite and calcite content in hydrated cementitious systems. *Mater. Struct.* **2017**, *50*, 680. [CrossRef]

49. Giammaria, G.; Lefferts, L. Catalytic effect of water on calcium carbonate decomposition. *J. CO2 Util.* **2019**, *33*, 341–356. [CrossRef]

50. Shahraki, B.K.; Mehrabi, B.; Gholizadeh, K.; Mohammadinasab, M. Thermal behavior of calcite as an expansive agent. *J. Min. Metall. Sect. B–Metall.* **2011**, *47*, 89–97. [CrossRef]

51. Schreiber, M.; Eckardt, M.; Klassen, S.; Adam, H.; Nalbach, M.; Greifenstein, L.; Kling, F.; Kittelmann, M.; Bechstein, R.; Kühnle, A. How deprotonation changes molecular self-assembly–an AFM study in liquid environment. *Soft Matter.* **2013**, *9*, 7145–7149. [CrossRef]

52. Turcanu, A.; Bechtold, T. pH Dependent redox behaviour of Alizarin Red S (1,2-dihydroxy-9,10-anthraquinone-3-sulfonate)–Cyclic voltammetry in presence of dispersed vat dye. *Dye. Pigment.* **2011**, *91*, 324–331. [CrossRef]

53. Li, Z.; Bowman, A.; Rayniak, A.; Xu, S. Anionic dye alizarin red S removal using heat-treated dolomite. *Crystals* **2024**, *14*, 187. [CrossRef]

54. Ramesh, T.N.; Kumari, T.M.; Kirana, D.V.; Ashwini, A.; Prathiba, J.M. Kinetics, thermodynamics and adsorption isotherm of alizarin red dye using calcium oxide. In *Proceedings of the National Conference on "Challenges and Opportunities for Chemical Sciences in 21st Century*; The National Academies Press: Washington, DC, USA, 2013; pp. 100–108.